

Research Highlights

Soft Matter

Ultrahigh-Density Hot Spots of Surface-Enhanced Raman Scattering

This report features the work of Ying-Huang Lai and his co-workers published in Adv. Func. Mater. 24, 2544 (2014).

According to recent work at Tunghai University in Taichung, hexagonal arrays of nanometer-spaced gold nanoparticles (NP) within a mesostructured polyoxo-methalate (POM)-silicatropic template (Au NP@PSS with POM sites) are suggested to be active three-dimensional (3D) substrates for surface-enhanced Raman scattering (SERS).¹ In *Advanced Functional Materials*, Ying-Huang Lai and co-workers reported that the size, narrow distribution of size and inter-particle distance of Au NP can be finely tailored within the PSS template as anion-exchange cycles enable the PSS to uptake gold ions continuously from the solution subphase for diffusion-controlled and POM-site-directed photochemical reduction inside the silica channels.¹ As revealed by X-ray diffraction, small-angle X-ray scattering and grazing-incidence small-angle X-ray scattering (SAXS) measured at BL23A at the TLS in the NSRRC, the Au NP directed by the PSS template were arrayed into a hexagonal lattice with a mean inter-channel spacing 3.2 nm and had a mean inter-particle spacing 2.8 nm along the channels (see Fig. 1).

Raman spectroscopy provide an important analytical tool to probe the chemical components and elements of materials. In particular, the discovery of SERS greatly enables sensitive detection of single molecules, making it possible to fingerprint molecules in tiny concentrations.² Two commonly accepted mechanisms of enhancement of SERS are an electromagnetic mechanism (EM) and a chemical mechanism (CM). EM that involves enhanced field intensity as a result of the excitation of surface plasmons results in a significantly increased cross section of Raman scattering. In general, EM occurs for molecules absorbed on metal colloids or a roughened metal surface; the enhancement of the EM

is roughly proportional to $|E|^4$ (10^6 - 10^8)— E denotes the intensity of the electromagnetic field. Arrays of metal nanoparticles, as an example, are among the most studied subjects for the EM of SERS.² Relative to EM, CM is an enhancement due to increased polarizability as charges transfer between a molecule and a substrate. The CM contribution to the non-resonant SERS enhancement is small (10 - 10^2). Graphene, as an example, has been intensively studied for large CM enhancement in SERS.³

In principle, these two mechanisms occur concurrently for molecules absorbed on the surface of metal NP, but the EM invariably dominates the enhancement of the Raman signals. In particular, when the gaps between metal particles, which are also known as hot spots, are less than 1 nm, the electromagnetic fields at the gaps become large. As a result, the Raman signals of the molecules located at the gap areas are greatly enhanced by hot spots. To date, numerous designs of two-dimensional (2D) SERS substrates such as arrays of metallic nanostructured objects or surfaces have been suggested, but simple 2D SERS substrates have limited sensitivity because of a limited number density of hot spots (typically less than 10^5 cm⁻³). To increase the sensitivity, 3D porous structures with large surface areas allowing the formation of hot spots are a good candidate.^{1,4} The narrowly spaced Au NP at PSS have an enormous number density (10^{19} NP cm⁻³) and can also provide densely packed hot spots for SERS.¹ These substrates allow the detection of 4-mercaptobenzoic acid (4-MBA) at a molecular level, down to 5 ng. Such a sensitive detection of 4-MBA molecules utilizing efficient 3D SERS substrates opens a path for affordable detection of chemical compounds in trace proportions.

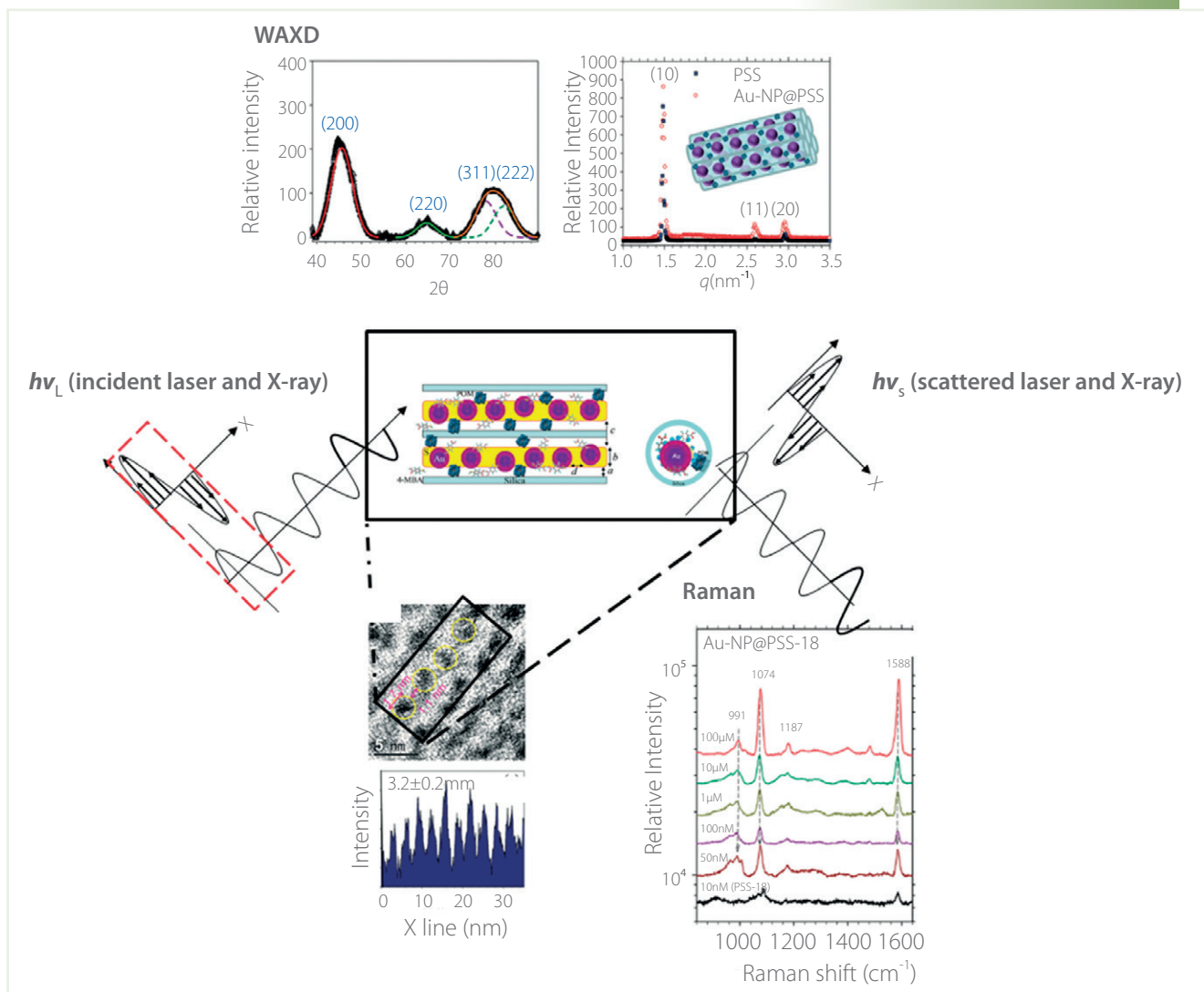


Fig. 1: Schematic of surface-enhanced Raman scattering of 4-MBA absorbed on Au-NP@PSS substrates. The mesostructures of PSS and crystals of Au NP were characterized with SAXS and WAXD. (Adapted from Ref. 1)

References

1. Y.-H. Lai, S.-W. Chen, M. Hayashi, Y.-J. Shiu, C.-C. Huang, W.-T. Chuang, C.-J. Su, H.-C. Jeng, J.-W. Chang, Y.-C. Lee, A.-C. Su, C.-Y. Mou, and U.-S. Jeng, *Adv. Func. Mater.* **24**, 2544 (2014).
2. K. Kneipp, M. Moskovits, and H. Kneipp (eds) *Surface-enhanced Raman Scattering - Physics and Applications* (Springer, 2006).
3. X. Ling, L. Xie, T. Fang, H. Xu, H. Zhang, J. Kong, M. S. Dresselhaus, J. Zhang, and Z. Liu, *Nano Lett.* **10**, 553 (2010).
4. H. Ko, S. Chang, and V. V. Tsukruk, *ACS Nano* **3**, 181 (2009).

How Can Sugar Connect with Electrical Memory?

This report features the work of Wen-Chang Chen, Redouane Borsali and their co-workers published in Adv. Funct. Mater. **24**, 4240 (2014).

Organic techniques address the energy and cost inefficiency issues posed by their inorganic counterparts. Organic (or carbon-based) electronics thus hold a

high promise of delivering cheap and energy-efficient materials and devices. Green materials are potentially an emerging concept within the carbon-based class

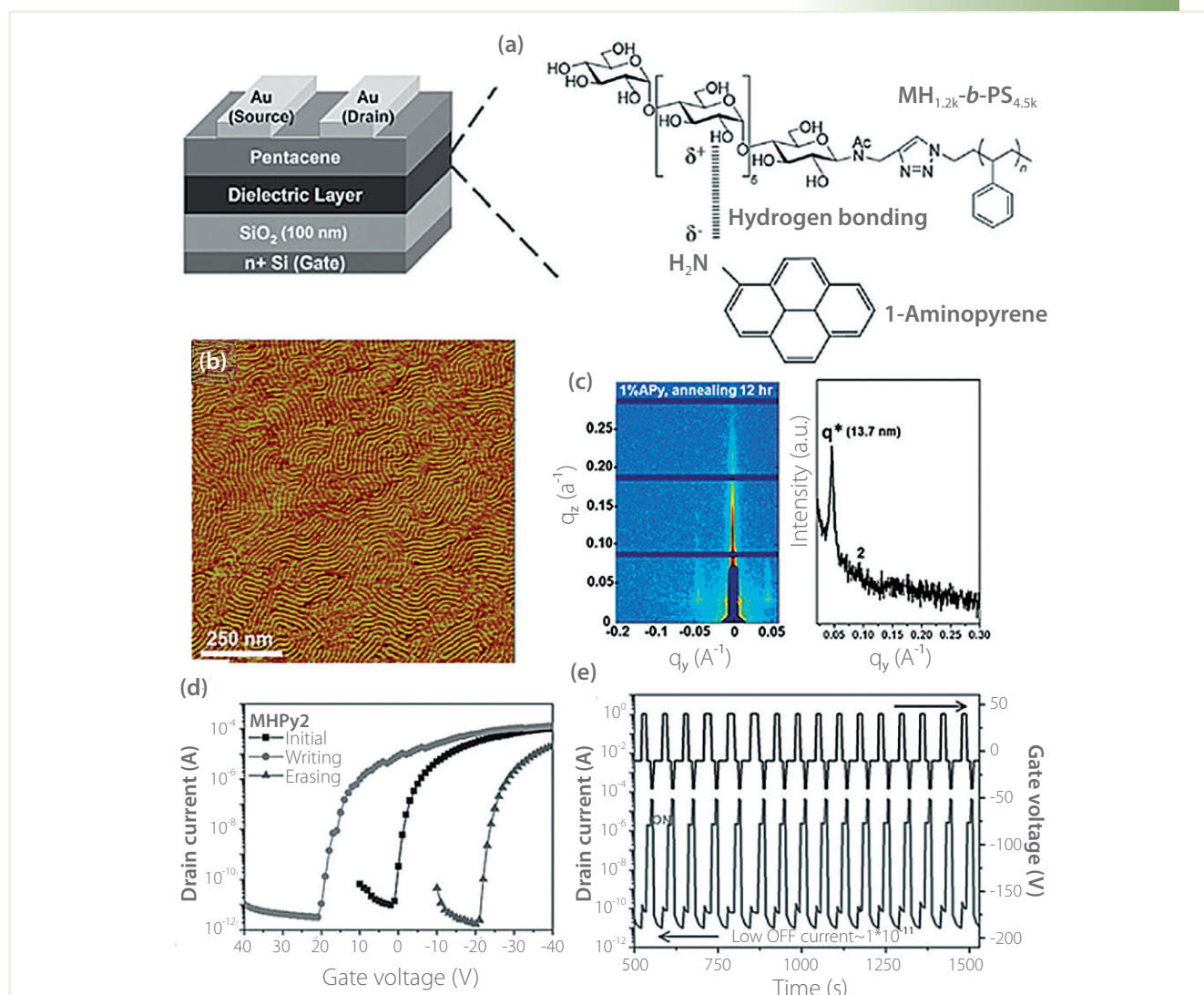


Fig. 1: (a) Schematic configuration of transistor memories based on supramolecular MH(Apy)-b-PS green electret; (b) AFM phase diagram, and (c) GISAXS patterns of a MH(Apy)-b-PS thin film annealed with H₂O/THF. (d) Transfer curve and (e) reversible switching between ON and OFF state in the transistor memory device. (Adapted from Ref.1)

towards achieving the goal of sustainability in the field of electronics. The exploration of such concepts is commonly hampered by the lack of active materials and processing strategies necessary to fabricate such green electronic devices. The cooperating research group between National Taiwan University and Centre de Recherches sur les Macromolécules Végétales (CERMAV, UPR-CNRS), led by Wen-Chang Chen and Redouane Borsali, respectively, reported a high-performance non-volatile transistor-memory green electret formed utilizing sugar-based block copolymers and their supramolecules.¹ The electret is composed of natural synthetic green block

copolymer maltoheptaose-*block*-polystyrene (MH-*b*-PS) supramolecules with 1-aminopyrene (APy) in small proportions, which is easily constructed to form nanoscale structures to integrate the tunneling layer and trapping element, as shown in Fig. 1(a). On choosing a suitable solvent vapor and duration of annealing, the strategies reported here could yield striking transitions in the secondary nanostructure of supramolecule thin films with varied APy loadings including sphere, vertical cylinder and horizontal cylinder; these are detected with grazing-incidence small-angle scattering (conducted at BL23A1 in the TLS) and AFM images (see representative data

in Fig. 1(b) and 1(c)), as the supramolecules were constructed on hydrogen-bonding APy to the MH moieties of a MH-*b*-PS.

The electrical memory performance is detectable from the transfer curves (Fig. 1(d)) and endurance cycles (Fig. 1(e)) operated at varied pulses of gate voltage. The hole-trapping capability of the device using a supramolecule electret with a horizontal cylinder structure was enhanced on increasing the APy composition; the excellent memory characteristics comprise a wide memory

window (52.7 V), long retention period, over 10^4 s, a large ON/OFF ratio, $>10^5$, and stable reversibility over 200 cycles without decay. The authors reveal a new approach to achieve a high-performance flash memory through the controlled morphology of sugar-based block copolymers and their supramolecules. (Reported by Cheng-Liang Liu, National Central University)

Reference

1. Y.-C. Chiu, I. Otsuka, S. Halila, R. Borsali, and W.-C. Chen, *Adv. Funct. Mater.* **24**, 4240 (2014).

Characteristic Morphologies of Conjugated Polymers for Photovoltaic Cells

This report features the work of Chi-An Dai, Leeyih Wang and their co-workers published in ACS Nano 8, 1254 (2014), Nanoscale 6, 2194 (2014), and Macromolecules 47, 5551 (2014).

Since polymers were discovered to conduct an electric current, remarkable progress has ensued in synthesizing conjugated polymers, in understanding their properties and in developing their application in photoelectronic devices. Conjugated polymers and their copolymers are regarded as most promising materials for new photovoltaic devices because of their excellent thermal and chemical stability, decreased costs and their tunable electronic and optical properties. Poly(3-hexylthiophene) (P3HT) has rapidly gained attention for use in organic solar cells, light-emitting diodes and thin-film transistors. The photoelectric properties of the fabricated devices are generally accepted to depend critically on the nanostructural forms of P3HT. To understand the kinetics of polymer crystallization and its correlation with morphological developments of conjugated polymers would hence provide notions about the optimal processing of future photovoltaic devices. Small-angle X-ray scattering (SAXS) and X-ray diffraction at TLS end stations **BL23A** and **BL13A** respectively captures the kinetics of conjugated polymer crystallization in the corresponding photovoltaic devices.

A research team comprising Chi-An Dai and Leeyih Wang at National Taiwan University and their associates has identified critical structural characteristics, polymorphic crystals and phase transformations in P3HT-based polymers, including nanohybrid,¹ rod-coil block copolymer² and rod-rod block copolymer,³ for solid-state dye-sensitized solar cells or photovoltaic devices. In the case of a P3HT/zinc oxide (ZnO) hybrid,¹ they proposed a synthetic method to fabricate *in situ* self-assembled organic and inorganic hybrid nanowires. This facile method can simultaneously organize P3HT chains and inorganic zinc precursors into highly ordered nanowires with length on a μm scale, followed by thermal oxidation to grow discrete ZnO nanocrystals directly on the existing P3HT nanowire template. After thermal annealing, the reorganization of the crystal structure of P3HT to yield chain axes highly oriented perpendicular to the fibril axis results in the segregation of ZnO nanocrystals into the surface of the crystalline P3HT nanowires to form a unique donor-acceptor parallel-lane nanowire network structure composed of alternating coextensive lanes of ZnO nanocrystals and P3HT nanowires that form the electron-acceptor channels (Figs. 1(a) and 1(c)). In Fig.

1(b), a grazing-incidence wide-angle scattering (GIWAXS) pattern exhibits intense arcs associated with the $(100)_{\text{P3HT}}$, $(200)_{\text{P3HT}}$ and $(300)_{\text{P3HT}}$ reflections along the q_z axis (substrate normal) and the $(020)_{\text{P3HT}}$ reflection along the q_{xy} axis (substrate parallel), indicating that the π -conjugated planes of P3HT block are parallel with respect to the substrate. Three diffraction maxima in higher q_{xy} were assigned to planes (100), (002), and (101) corresponding to the wurtzite structure of ZnO, confirming the presence of crystalline nanoparticles. On measuring the photovoltaic efficiency of P3HT/ZnO hybrid devices, they found that the donor-acceptor parallel-channel structure gave access to improved dissociation of excitons and charge transport, thereby enhancing quenching of photoluminescence, charge transport and device performance. The photovoltaic devices with a donor-acceptor parallel-lane structure of P3HT/ZnO hybrid gave PCE 0.61% relative to only 0.07% from a conventional P3HT/ZnO bulk heterojunction solar cell.

On investigation of poly(3-hexyl thiophene)-*b*-

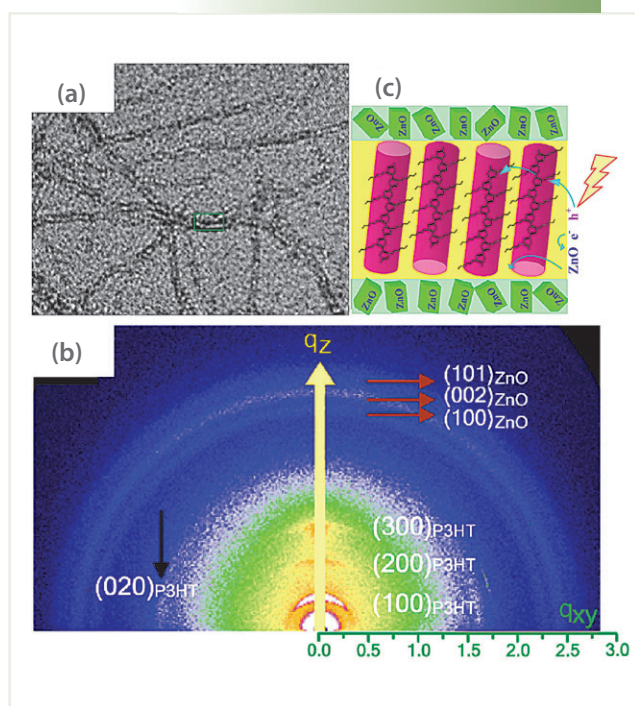


Fig. 1: (a-b) TEM micrograph and GIWAXS pattern of P3HT/ZnO hybrid. (c) Cartoon for a donor-acceptor parallel-lane nanowire structure. PTh₄BT and PTh₄FBT before and after thermal annealing. (Reproduced from Ref. 1)

poly(2-vinyl pyridine) P3HT-*b*-P2VP,² they reported a new approach to control the polymorphs and nanostructures of the copolymer for future applications using processing in solution and subsequent thermal treatment. Figures 2(a)-2(b) show the temperature-dependent profiles of SAXS and wide-angle X-ray scattering (WAXS) from *in situ* measured during a step-wise heating course. In the WAXS profiles (Fig. 2(b)), observed diffraction maxima at $(100)_{\parallel}$, $(200)_{\parallel}$ and $(020)_{\parallel}$ below 80 °C indicated the self-assembly in solution of P3HT-*b*-P2VP first formed from II crystals of P3HT within its nanofibrillar core confined by P2VP blocks in the surrounding domain. Distinct from a mixture of form-I and form-II crystals in a P3HT homopolymer, the formation of the rare form-II crystals is attributed mainly to the consequence of a slow crystallization of the P3HT block under the nanoconfinement imparted by neighboring P2VP blocks along the crystal growth during drying. With increasing temperature and then cooling, a new phase transformation from form-II crystals to form-I crystals is observed in Fig. 2(b). Upon heating the sample further

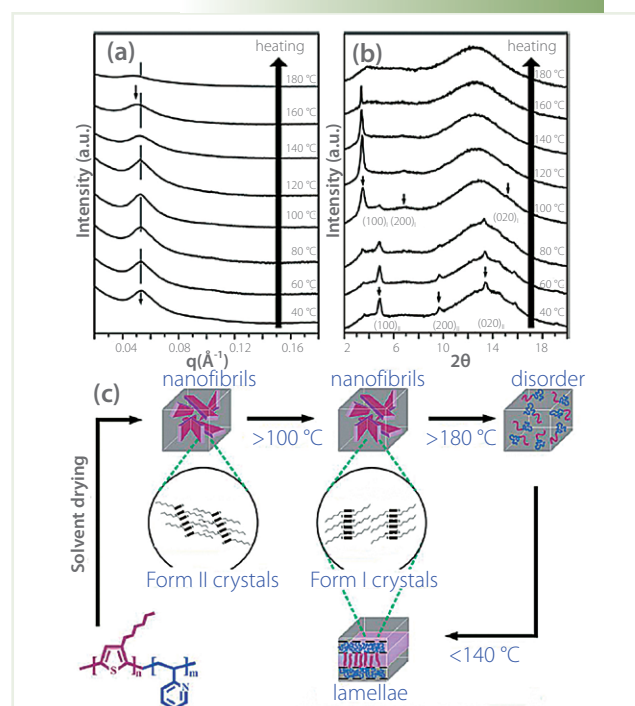


Fig. 2: (a, b) SAXS and WAXS profiles for the solvent-cast sample of P3HT-*b*-P2VP on step-wise heating; (c) Cartoon for the route of phase transformations of solution-dried P3HT-*b*-P2VP. (Reproduced from Ref. 2)

to 120 °C, new sharp and intense diffraction signals associated with planes (100)_i and (020)_i emerge, showing the phase transformation from form-II crystals to form-I crystals. At temperature 160 °C, the WAXS profiles correspond to weak (100) diffraction, indicating a nematic liquid-crystalline structure of P3HT. Figure 2(c) illustrates schematically the structural evolution and phase transformation including the mesoorder–disorder, order–order and polymorphism transitions from a solvent-cast sample of P3HT-*b*-P2VP.

These workers synthesized poly(2,5-dihexyloxy-*p*-phenylene)-*b*-poly(3-hexylthiophene) (PPP-*b*-P3HT) and applied it as a material for hole transport (HTM) in dye-sensitized solar cells.³ WAXS profiles in Fig. 3 show diffraction signals for PPP-*b*-P3HT block copolymer and two homopolymers of PPP and P3HT. The PPP-*b*-P3HT exhibits diffraction signals (100), (200) and (300) similar to those obtained from the crystalline P3HT homopolymer, whereas no diffraction signal in the WAXS profile was

associated with PPP for the copolymer. These observations clearly verify that the P3HT segments in the block copolymer tend to form a crystalline supramolecular structure through π - π stacking of the P3HT during the spin drying, but the PPP block remains an amorphous structure. From measurements of transient photovoltage, they found that the photovoltaic cell based on PPP-*b*-P3HT as a HTM has a greater electron lifetime than that of the reference device based on P3HT homopolymer. These findings indicated that amorphous PPP segments in the copolymer improve the molecular packing of the P3HT blocks to form interpenetrating fibrils with long-range order during spin drying, leading to a hole mobility for the block copolymer greater than that of the parent P3HT homopolymer with a comparable molar mass. Moreover, the PPP chain significantly improves both the completeness and tightness of the HTM coverage on top of the sensitized titania such that the probability of carrier recombination is decreased, yielding a significant advance in photovoltaic performance.

In summary, their new findings a detailed understanding of the dependence of self-assembly of P3HT based polymers on both kinetic and thermodynamic effects and offer guidance for the morphological control and optoelectronic properties in the device applications. (Reported by Wei-Tsung Chuang)

References

1. Y. H. Lee, Y. P. Lee, C. J. Chiang, C. Shen, Y. H. Chen, L. Wang, and C. A. Dai, *Macromolecules* **47**, 5551 (2014).
2. Y. H. Lee, Y. L. Yang, W. C. Yen, W. F. Su, and C. A. Dai, *Nanoscale* **6**, 2194 (2014).
3. W. C. Chen, Y. H. Lee, C. Y. Chen, K. C. Kau, L. Y. Lin, C. A. Dai, C. G. Wu, K. C. Ho, J. K. Wang, and L. Wang, *ACS Nano* **8**, 1254 (2014).

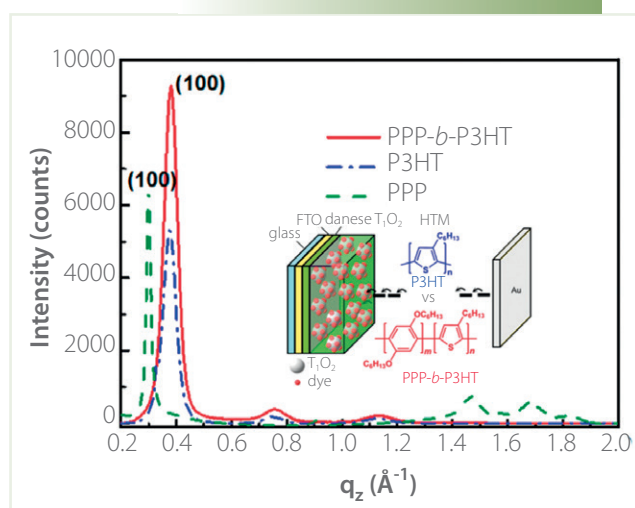


Fig. 3: WAXS profiles of PPP-*b*-P3HT, P3HT and PPP films. (Reproduced from Ref. 3)